ALGORITMO DE FUSIÓN DE IMÁGENES ESPECTRALES EN EL DOMINIO COMPRIMIDO PARA EL AUMENTO DE LA RESOLUCIÓN ESPACIOESPECTRAL

ÓSCAR JAVIER ESPITIA MENDOZA

UNIVERSIDAD INDUSTRIAL DE SANTANDER

FACULTAD DE INGENIERÍAS FÍSICO-MECÁNICAS

ESCUELA DE INGENIERÍA DE SISTEMAS E INFORMÁTICA

BUCARAMANGA

2017

ALGORITMO DE FUSIÓN DE IMÁGENES ESPECTRALES EN EL DOMINIO COMPRIMIDO PARA EL AUMENTO DE LA RESOLUCIÓN ESPACIOESPECTRAL

ÓSCAR JAVIER ESPITIA MENDOZA

Trabajo de investigación para optar al título de:

Magíster en Ingeniería de Sistemas e Informática

Director:

HENRY ARGUELLO FUENTES

Ingeniero Electricista, Ph.D

UNIVERSIDAD INDUSTRIAL DE SANTANDER

FACULTAD DE INGENIERÍAS FÍSICO-MECÁNICAS

ESCUELA DE INGENIERÍA DE SISTEMAS E INFORMÁTICA

BUCARAMANGA

2017

CONTENTS

LIST OF FIGURES

LIST OF TABLES

List of Abbreviations

CS	**C**ompressive **S**ampling
HS	**H**yperspectral
MS	**M**ultispectral
CASSI	**C**oded **A**perture **S**napshot **S**pectral **I**mager
SSCSI	**S**patio-**S**pectral **E**ncoded **C**ompressive **S**pectral **I**mager
HR	**H**igh **R**esolution
ADMM	**A**lternating **D**irection**M**ethoid of **M**ultipliers

List of Symbols

Variable notatios

$\mathbf{f}$	Reference image
$\mathbf{\Phi}$.	Measurement matrix
$\mathbf{\Psi}$	Sparsity operator
$\boldsymbol{\mathcal{L}}$	Smoothness operator
$\mathbf{x}$	Sparse version of $\mathbf{f}$
$\mathbf{y}$.	Compressed measurements
$\mathbf{n}$	Noise
$\mathbf{L}$	Spatial downsampling operator
$\mathbf{B}$	Spectral blurring operator
$.^T$	Transpose operator

Size notatios

M	number of rows
N	number of columns
L	number of spectral bands
N_H	Size of the reference
p	Spatial decimation factor
q	Spectral decimation factor

Mathematical symbols

$\ll$	Much lower
$\gg$	Much greater
$\otimes$	Kronecker product

$||\cdot||_1$ ℓ_1 norm

$||\cdot||_2$ ℓ_2 norm

RESUMEN

TÍTULO: ALGORITMO DE FUSIÓN DE IMÁGENES ESPECTRALES EN EL DOMINIO COMPRIMIDO PARA EL AUMENTO DE LA RESOLUCIÓN ESPACIOESPECTRAL *

AUTOR: Óscar Javier Espitia Mendoza **

PALABRAS CLAVE: Fusión de imágenes , Imágenes espectrales, Muestreo compresivo.

Los sensores de compresión de imágenes espectrales reducen el número de píxeles muestreados mediante la combinación de información espectral codificada de una escena en proyecciones bidimensionales. Sin embargo, el muestreo de datos comprimidos con alta resolución espacial y alta resolución espectral, simultaneamente, demanda la disposición de sensores de alta resolución, que pueden ser costosos. Este trabajo introduce un modelo que permite fusionar información de diferentes sensores de compresión con alta resolución espacial, pero baja resolución espectral, con la de sensores de alta resolución espectral, pero baja resolución espacial. Basado en este modelo, el proceso de fusión de medidas comprimidas es formulado como un problema inverso; que minimiza una función objetivo definida como la suma de términos cuadráticos de fidelidad con los datos, y terminos de penalización por suavidad y baja densidad; que es resuelto siguiendo el espíritu del método de dirección alternada de multiplicadores (ADMM, de su sigla en inglés). Los parámetros de los diferentes sensores son optimizados y el principio de baja densidad es estudiado para mejorar la calidad de las reconstrucciónes. Los resultados de las simulaciones con datos reales y simulados, con diferentes sistemas de compresión de imágenes, permmiten apreciar la calidad del método de fusión propuesto.

*Trabajo de investigación

**Facultad de Ingenierías Físico-mecánicas. Escuela de Ingeniería de sistemas e informática. Director, Henry Arguello Fuentes.

ABSTRACT

TITLE: SPECTRAL IMAGE FUSION ALGORITHM FOR INCREASING SPATIOSPECTRAL RESOLUTION FROM COMPRESSIVE MEASUREMENTS *

AUTHOR: Óscar Javier Espitia Mendoza **

KEYWORDS: Image fusion , Spectral imaging, compressive sensing.

Compressive spectral imagers take a reduced number of sampled pixels by coding and combining the spectral information of a scene in a single two-dimensional projection. Sampling compressed information with simultaneous high spatial and high spectral resolution demands expensive high-resolution sensors, however, the high resolution is a latent requirement in remote sensing applications, and also a very important issue in this area. This work introduces a model allowing compressed data from high spatial/low spectral and low spatial/high spectral resolution sensors to be fused. Based on this model, the compressive fusion process is formulated as an inverse problem that minimizes an objective function defined as the sum of quadratic data fidelity terms, smoothness and sparsity regularization penalties, which is solved by following the spirit of the Alternating Direction Method of Multipliers (ADMM), which is an adequate procedure for large-scale problems such as this. The parameters of the different sensors are optimized and the sparsity prior is studied, thus, it is introduced a measurement matrix optimization procedure in order to improve the quality of reconstructions. Simulation results conducted on synthetic and real data, with different CS imagers, allow the quality of the proposed fusion method to be appreciated in relation to other approaches.

*Research Work

**Faculty of Physical-Mechanical Engineering. Department of Systems Engineering and Informatics. Advisor, Henry Arguello Fuentes.

INTRODUCTION

CONTEXT AND OBJECTIVES OF THE THESIS

Background: Hyperspectral imaging allows an accurate identification of the sensed materials via spectroscopic analysis, facilitating several applications such as Earth observation, remote sensing, food safety, pharmaceutical process monitoring and quality control, as well as biomedical, industrial, and forensic applications Bioucas-Dias et al., 2013; Xiong et al., 2014; Bellante et al., 2013; Lu and Fei, 2014; Ryan et al., 2014. The extraction of useful information from hyperspectral images involves sophisticated inference methods trying to overcome the problems related to the high dimensionality of these images and to their low spatial resolution. These methods often require the resolution of inverse problems that are considered in many research topics, including compressive acquisition, super-resolution, and fusion (see Bioucas-Dias et al., 2013 for descriptions).

Remote sensing imagers usually deliver images with either high spatial/low spectral or high spectral/low spatial resolutions. However, applications involving feature detection, tracking, and classification require images with both high spectral and high spatial resolutions Bioucas-Dias et al., 2013. On the other hand, most imaging systems deliver data with a significant redundancy, which can be reduced by using compressive sampling (CS) Arce et al., 2014; Arguello and Arce, 2014. CS is based on the fact that many natural signals can be represented with a few coefficients in some basis and can thus be efficiently compressed. It has been shown that the use of appropriate sensing matrices allows the performance of signal reconstruction methods to be close to the one obtained without using CS Candes and Wakin, 2008. However, designing systems characterized by low-cost compressed measurements

with high spatial and high spectral resolutions is still a challenging problem.

There are several approaches for compressing spectral data. This work focusses on two classes of imagers that have been implemented in practical applications: i) spatial coding-based CS imagers, such as the Coded Aperture Snapshot Spectral Imager (CASSI) Wagadarikar et al., 2008 and ii) spectral coding-based spectral imagers, such as the Spatio-spectral Encoded Compressive Spectral Imager (SSCSI) Lin et al., 2014, or the Colored-CASSI Arguello and Arce, 2014. At this point, it is interesting to mention that other theoretical approaches have been studied for compressive spectral imaging, such as the Hyperspectral Coded Aperture (HYCA) Martín, Bioucas-Dias, and Plaza, 2015 or the Compressive-projection Principal Component Analysis Fowler, 2009. However, these approaches have, to the author knowledge, never been applied in practical applications.

Problem Formulation (Matrix-vector form): This work introduces a model allowing high-resolution spectral images to be reconstructed from two images with different spatial and spectral resolutions acquired with compressive spectral imagers. The observed images are assumed to result from spectral and/or spatial degradations of a high spectral and high spatial resolution hyperspectral (HS) image (to be recovered) acquired with a CS operation. The HS image of interest is stacked into a column vector $\mathbf{f} = [f_1, ..., f_{N_H}]^T \in \mathbb{R}^{N_H}$, where $N_H = MNL$, MN is the number of image pixels and L is the number of spectral bands. We also assume that $\mathbf{f}$ can be decomposed as $\mathbf{f} = \mathbf{\Psi x}$, where $\mathbf{x} \in \mathbb{R}^{N_H}$ contains only $N_z \ll N_H$ nonzero elements and $\mathbf{\Psi} \in \mathbb{R}^{N_H \times N_H}$ is an operator expressing the fact that the image is sparse in a given domain. This decomposition assumes that the image of interest can be described as a linear combination of a few atoms belonging to the dictionary $\mathbf{\Psi}$. The choice of the dictionary $\mathbf{\Psi}$ is crucial for many applications. Two strategies have been investigated in the literature: i) the dictionary can be constructed using pre-defined

bases such as Wavelets, Curvelets Rubinstein, Bruckstein, and Elad, 2010 or ii) can be learned from the data using dictionary learning techniques Tosic and Frossard, 2011. Both approaches will be investigated in this work.

The noiseless observations considered in this work are HS and multispectral (MS) compressed images denoted as $\mathbf{f}_H = \mathbf{\Phi}_1\mathbf{B}\mathbf{f} = \mathbf{\Phi}_H\mathbf{f}$ and $\mathbf{f}_M = \mathbf{\Phi}_2\mathbf{L}\mathbf{f} = \mathbf{\Phi}_M\mathbf{f}$, where $\mathbf{B} \in \mathbb{R}^{M_hN_hL\times N_H}$ $(M_hN_h \ll MN)$ is an operator associated with spatial blurring and downsampling, $\mathbf{L} \in \mathbb{R}^{MNL_m\times N_H}$ $(L_m \ll L)$ is a filtering operator transforming the spectral content of the reference image into the spectral bands of the MS image, $\mathbf{\Phi}_1 \in \mathbb{R}^{P\times M_hN_hL}$ and $\mathbf{\Phi}_2 \in \mathbb{R}^{Q\times NML_m}$ are appropriate sensing matrices. Thus, $\mathbf{\Phi}_H = \mathbf{\Phi}_1\mathbf{B} \in \mathbb{R}^{P\times N_H}$ and $\mathbf{\Phi}_M = \mathbf{\Phi}_2\mathbf{L} \in \mathbb{R}^{Q\times N_H}$ are the respective HS and MS CS matrices that perform both compression and decimation operations, simultaneously. In summary, the observation model adressed in this work follow from

$$\begin{aligned}\mathbf{y}_H =& \mathbf{\Phi}_H\mathbf{f} + \mathbf{n}_H\\ \mathbf{y}_M =& \mathbf{\Phi}_M\mathbf{f} + \mathbf{n}_M\end{aligned} \tag{1}$$

The problem addressed in this work is the estimation of the HR image $\mathbf{f}$ (assumed to be sparse in the $\mathbf{\Psi}$ domain) from the noisy measurements $\mathbf{y}_H = \mathbf{f}_H + \mathbf{n}_H$ and $\mathbf{y}_M = \mathbf{f}_M + \mathbf{n}_M$, where $\mathbf{n}_H$ and $\mathbf{n}_M$ are the HS and MS noise vectors Candes and Wakin, 2008; Arguello and Arce, 2014; Arce et al., 2014. Notice that the observation model defined by $\mathbf{y}_H$ and $\mathbf{y}_M$ is similar to the one introduced in Wei et al., 2015, except that the unknown image $\mathbf{f}$ has been vectorized. However, an important difference with respect to Wei et al., 2015 is that the observed images have been compressed leading to a reduced cost for their acquisition. The main objective of this work is to show that we can exploit sparsity to fuse compressed spectral images. Notice that sparsity guarantees that the inverse problem consisting of estimating $\mathbf{f}$ from $\mathbf{y}_H$ and

$\mathbf{y}_M$ is well-posed Needell and Ward, 2013.

The problem of fusing multi-resolution images has received much attention in the literature Wei, Dobigeon, and Tourneret, 2015; Wei et al., 2015; Wei et al., 2016. Some recent works have also been devoted to the fusion of compressive data in order to increase the interpretability of the images Luo et al., 2010; Yin et al., 2015. We argue that the use of compressive measurements with appropriate sensing matrices can lead to high-quality image reconstruction and that compressive measurements have favorable properties to solve the multisensor fusion problem. Based on the above discussion, we propose to formulate the fusion problem as an inverse problem that minimizes an appropriate objective function. This function is classically built as the sum of quadratic data fidelity terms and a penalty term, such as

$$\hat{\mathbf{f}} = \arg\min_{\mathbf{f}} ||\mathbf{y}_H - \mathbf{\Phi}_H \mathbf{f}||_2^2 + ||\mathbf{y}_M - \mathbf{\Phi}_M \mathbf{f}||_2^2 + \phi(\mathbf{f}) \tag{2}$$

Objective: To address the challenging problem of superresolution and fusion of images with degradations in different ways involves the analysis and to develop innovative procedures to reconstruct images with high resolution.

In this thesis, we propose to exploit the compressive acquisition process of the different images. More precisely, the sensor specifications (i.e., spectral or spatial responses and compression) are exploited to properly design the spatial or spectral degradations suffered by the image to be recovered.

In particular, the high spatial resolution HS image to be estimated is assumed to live in a lower dimensional subspace, which is a suitable hypothesis when the observed scene is composed of a finite number of macroscopic materials, furthermore, allow the measurements to be compressed.

The fusion problem is incorporated into the model which follow the spirit of the Alternating Direction Method of Multipliers, then a splitting procedure has to be designed carefully, also the regularization parameters. All these points will have to account in this thesis.

ORGANIZATION OF THE MANUSCRIPT

- **Chapter 1**: This chapter is interested in the state of the art compressive imagers, especially, they who have a practical implementation. Theoretical approaches, which will be ideal references for the results, also are mentioned. Several parameters of these sensors are studied in order to design an information fusion procedure.

- **Chapter 2**: This chapter presents a description of the imagers which produce the images to be fused, from their matrix model. Also, it presents a matrix design procedure, in order to take advantage of the information from each source, efficiently, which will be tested in order to increase the accurate in reconstructions.

- **Chapter 3**: This chapter focuses on the develop of the algorithm to fuse CS measurements and reconstruct high-resolution spectral images, it depicts the ADMM approach used to solve the inverse problem studied in this work, and details how each parameter is updated and different rules to do it.

- **Chapter 4**: This chapter presents the design of the simulations and the respective results, which show the efficiency of the proposed compressive fusion approach.

MAIN CONTRIBUTIONS

- **Chapter 1**: A short review of the compressive spectral imagers, which follows from a collaboration of a review paper of the main compressive spectral imagers Medina, H.Arguello, and Gómez, 2017.
- **Chapter 2**: Matrix design idea from the mutual coherence principle, applicable to compressive imagers with practical implementation.
- **Chapter 3**: Algorithm to fuse compressive measurements from different sources to increase the spectral image resolution, based on the ADMM principles.

LIST OF PUBLICATIONS

Papers in preparation

o Ó. Espitia, H. Arguello, J-Y. Tourneret. “Spectral Image Fusion from Compressive Measurements”

Conference papers

o Ó. Espitia ; S. Castillo ; H. Arguello; Compressive hyperspectral and multispectral imaging fusion . Proc. SPIE 9840, Algorithms and Technologies for Multispectral, Hyperspectral, and Ultraspectral Imagery XXII, 984023 (May 17, 2016); doi:10.1117/12.2224268.

o H. Garcia, Ó. Espitia and H. Arguello, "Multiresolution spectral imaging by combining different sampling strategies in a compressive imager, MR-CASSI," 2016 XXI Symposium on Signal Processing, Images and Artificial Vision (STSIVA), Bucaramanga, 2016, pp. 1-6. doi: 10.1109/STSIVA.2016.7743325

- (Submitted conference) Ó. Espitia, H. Arguello, J-Y. Tourneret. “High-resolution spectral image reconstruction based on compressed data fusion”

Other publications related to previous works

- L. Lopez, O. Espitia and H. Arguello, "Localized X-ray compressive computer tomography reconstruction by designing measurement matrix," 2016 XXI Symposium on Signal Processing, Images and Artificial Vision (STSIVA), Bucaramanga, 2016, pp. 1-5. doi: 10.1109/STSIVA
.2016.7743316.

- (Submitted conference) M. Calderón, Ó. Espitia, D. Molina, H. Arguello.“2D-Nuclear magnetic resonance spectra recovery from subsampled measurements based on a separable optimization problem”, EUSIPCO 2017, (As a result of undergraduate thesis co-advice)

1. BACKGROUND ON COMPRESSIVE SPECTRAL IMAGERS

1.1. INTRODUCTION

This work focusses on two classes of imagers that have been implemented in practical applications, first, those spatial coding-based CS imagers, such as the Coded Aperture Snapshot Spectral Imager (CASSI) Wagadarikar et al., 2008, and second, those spectral coding-based spectral imagers, such as the Spatio-spectral Encoded Compressive Spectral Imager (SSCSI) Lin et al., 2014, or the Colored-CASSI Arguello and Arce, 2014. Also, it is interesting to mention that other theoretical approaches have been studied for compressive spectral imaging, such as the Hyperspectral Coded Aperture (HYCA) Martín, Bioucas-Dias, and Plaza, 2015 or the Compressive-projection Principal Component Analysis Fowler, 2009. However, these approaches have, to the author knowledge, never been applied in practical applications.

1.2. SPATIAL CODING BASED CS IMAGER: CASSI

CS imagers capture a spectral scene using 2D projections that are obtained with different sampling patterns. For instance, the coded aperture snapshot spectral imager (CASSI) system uses a coded aperture that replaces the entrance slit of a dispersive spectrometer by a much wider field stop, inside which is inserted a binary-coded mask. This mask attempts to create a transmission pattern. The encoded light, transmitted by the coded mask within the field stop, is then passed through a standard spectrometer back-end (i.e., collimating lens, disperser, reimaging lens, and detector array). This compression procedure is illustrated in Fig. 1.

Figure 1: Compression with spatial coding. The spectral scene is coded and dispersed by a dispersive element (grating or prism). Thus, the detector creates a 2D projection of the coded and shifted scene.

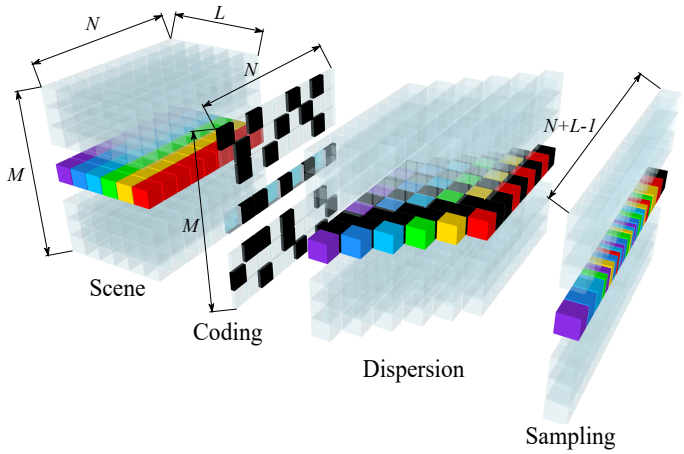

The CASSI projections can be discretized as

$$\mathbf{g}^k = \mathbf{\Phi}^k \mathbf{f} \tag{1.1}$$

where $k = 1, ..., K$ corresponds to the kth single snapshot acquired with a sampling pattern $\mathbf{T}^k \in \mathbb{R}^{M \times N}$, $\mathbf{g}^k \in \mathbb{R}^{M(N+L-1)}$ contains the measurement stacked into a column vector, $\mathbf{f} \in \mathbb{R}^{MNL}$ contains the values of the discrete source spectral density, and $\mathbf{\Phi}^k \in \mathbb{R}^{M(N+L-1)\times(MNL)}$ is the sparse modulation matrix of the kth CASSI snapshot (that performs both coding and shifting operations, as mentioned before). The matrix $\mathbf{\Phi}$ has ideally binary entries, as illustrated in Fig. 2. Note that its structure consists of a set of diagonal patterns, that repeat along the horizontal direction, such that one spatial dimension is shifted downward, as many times as the number of spectral bands. Each diagonal element is due to the sampling pattern $\mathbf{T}$, that has been vectorized column-wise. Note that other patterns of diagonal elements are vertically stacked when several snapshots are considered by the system.

Figure 2: CASSI coded projection operator (for capturing 4 spectral bands by using 2 different sampling patterns in 2 snapshots).

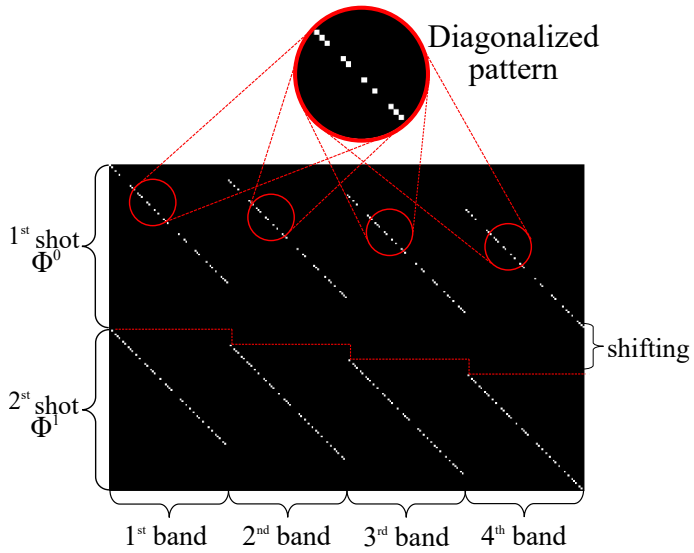

1.3. SPATIO-SPECTRAL CODING BASED CS IMAGER: SSCSI

Another state-of-the-art compressive imager is the spatio spectral encoded compressive spectral imager (SSCSI). Here, the coded sensor image is achieved by applying a diffraction grating to disperse the light into the spectrum plane and inserting a coded attenuation mask between the spectrum plane and the sensor plane. The diffraction grating on the image plane maps the spectral dimension of the light to its angular dimension. A ray incident on the diffraction grating produces multiple diffracted outgoing rays in different directions with different spectral bands, as illustrated in Fig. 3.

Figure 3: Compression with spectral coding.

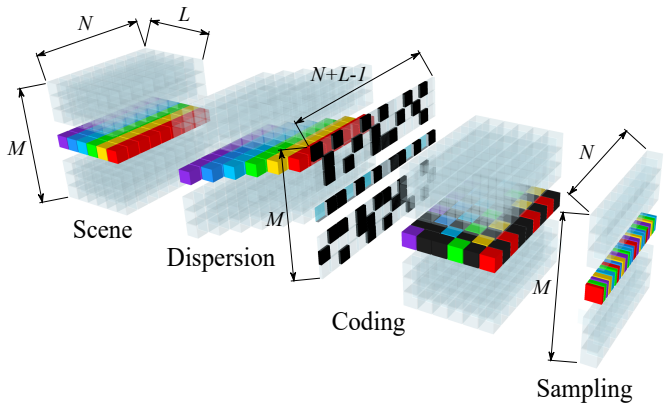

The compression procedure of the SSCSI can also be discretized as in (1.1), i.e., as $\mathbf{g}^k = \mathbf{\Phi}^k \mathbf{f}$, where $\mathbf{g}^\ell \in \mathbb{R}^{MN}$ is the kth vertorized sensor image, and $\mathbf{\Phi}^k \in \mathbb{R}^{MN \times MNL}$ is the modulation matrix. The L vectorized spectral bands, stacked in a column vectror, are modulated by each modulation matrix $\mathbf{\Phi}^k \in \mathbb{R}^{MN \times MNL}$, which contains the sheared pattern from the mask $\mathbf{T}^k \in \mathbb{R}^{M \times (N+L-1)}$ on its diagonal. The resulting sparse modulation matrix with binary entries is displayed in Fig. 4. Note that it is also structured as a set of diagonal patterns. However, the patterns do not repeat horizontally, allowing spectral coding.

Figure 4: SSCSI coded projection operator (for capturing 4 spectral bands by spectral coding in 1 snapshot).

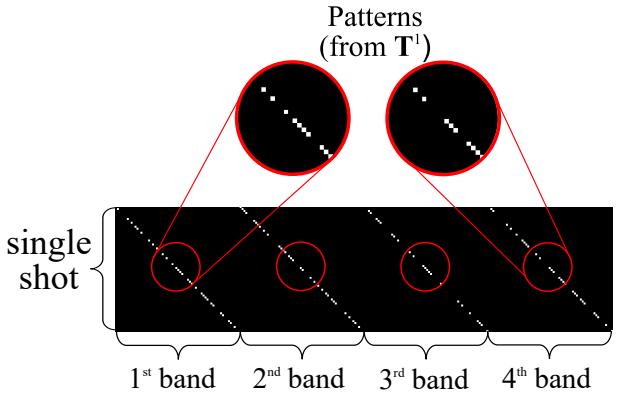

1.4. GAUSSIAN MEASUREMENT MATRICES

Some CS systems compute a few random projections of the observations using, e.g., Gaussian independent and identically distributed (i.i.d.) vectors allowing spatial/spectral coding Martín, Bioucas-Dias, and Plaza, 2015; Fowler, 2009. These systems have proved their efficiency for data reconstruction and will be used as a benchmark compared with the proposed methods. These systems can be also described by the matrix-vector form of (1.1). However, the coded projection operator is expressed as a sparse modulation matrix with Gaussian entries, as illustrated in Fig. 5. Note that the sensing matrix in Fig. 5 is built using diagonal Gaussian vectors.

Figure 5: Gaussian coded projection operator (for capturing 4 spectral bands by using i.i.d. vectors as sampling patterns)

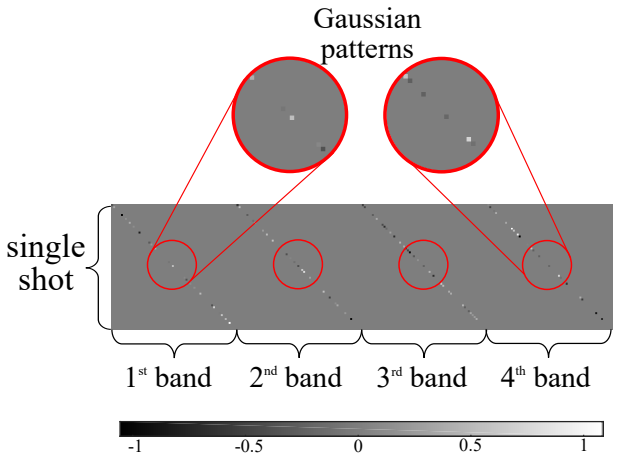

2. MEASUREMENT MATRIX FOR CS IMAGE FUSIÓN

2.1. INTRODUCTION

The structure of the sensing matrices $\mathbf{\Phi}_H$ and $\mathbf{\Phi}_M$ can have a strong impact on the quality of the reconstructed images. This section recalls the constraints associated with these matrices for the CASSI system.

2.2. STRUCTURE OF THE SENSING MATRICES IN THE CASSI SYSTEM

This section shows that the structure of each measurement matrix depends on the sampling patterns and it will be stated as a function of them. Fig. 6 shows the structure of the HS sparse modulation matrix $\mathbf{\Phi}_H$. Note that each row of this matrix performs a linear combinations of p^2 adjacent pixels, which means that the scene projected onto this matrix, besides being compressed, will be degraded spatially by a factor p (e.g., $p = 2$ in Fig. 6). More specifically, the entries of the matrix $\mathbf{\Phi}_H$ are defined as

$$\Phi_{H_{i,j}} = \begin{cases} t_H\left(a_j + \frac{M}{p} b_j + \frac{M^2}{p^2} c_j\right) & \text{if } i = a_j + \frac{M}{p}(b_j + c_j) \\ 0 & \text{otherwise} \end{cases} \tag{2.1}$$

where $\boldsymbol{t}_H = [t_H(1), ..., t_H(\frac{MN}{p^2})]^T$ is the vectorized coded aperture $\mathbf{T}$ of the HS imager, $a_j = \lfloor \frac{j}{q} \rfloor$, $b_j = \lfloor \frac{j}{qM} \rfloor - \lfloor \frac{j}{M} \rfloor$, $c_j = \lfloor \frac{j}{M^2} \rfloor$ and $\lfloor . \rfloor$ denotes the integer part. Note that that the matrix $\mathbf{\Phi}_H$ is fully characterized by the vector $\boldsymbol{t}_H$.

Figure 6: HS CASSI measurement matrix $\mathbf{\Phi}_H$.

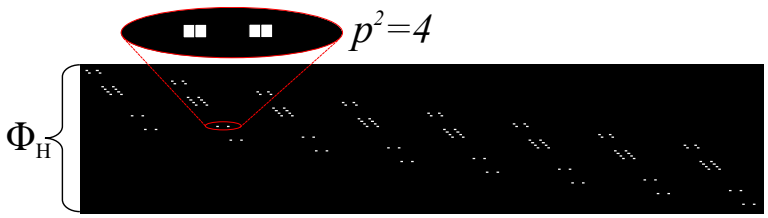

Similarly, Fig. 7 shows the structure of the CASSI sensing matrix $\mathbf{\Phi}_M$ used for the MS measurements. Note that each row of this matrix performs a linear combination between the pixels of the q adjacent bands, which means that the spectral resolution of the MS sensor is q times smaller than the one of the reference scene (e.g., $q = 4$ in Fig. 7). More precisely, the entries of the matrix $\mathbf{\Phi}_M$ can be written as follows

$$\Phi_{M_{i,j}} = \begin{cases} t_M\big(i - r_j(MN - M)\big) & \text{if } i = j \bmod(NM) + M\lfloor \frac{j}{qMN} \rfloor \\ & \text{and } j - r_j M \geq 0 \\ 0 & \text{otherwise} \end{cases} \tag{2.2}$$

where $\boldsymbol{t}_M = [t_M(1), ..., t_M(NM)]^T$ is the vectorized coded aperture $\mathbf{T}$ of the MS imager and $r_j = \lfloor \frac{j}{MN} \rfloor$. Note that that the matrix $\mathbf{\Phi}_M$ is fully characterized by the vector $\boldsymbol{t}_M$.

Figure 7: MS CASSI measurement matrix $\mathbf{\Phi}_M$.

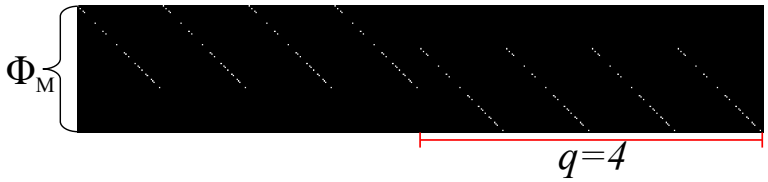

The design of the matrices $\mathbf{\Phi}_H$ and $\mathbf{\Phi}_M$ is the objective of the next section.

2.3. SENSING MATRIX DESIGN

In CS theory, a suitable measurement matrix $\mathbf{\Phi}$ is desired to be as incoherent as possible with the sparse dictionary $\mathbf{\Psi}$ Candes and Wakin, 2008. The mutual coherence of the Gram matrix $\mathbf{G} = (\mathbf{\Phi\Psi})^T(\mathbf{\Phi\Psi})$ is defined as the off-diagonal entry in $\mathbf{G}$ with the largest absolute magnitude. The sensing matrix can be optimized by minimizing the mutual coherence the $\mathbf{G}$. Consequently, considering that the dictionary is known, a sensing matrix can be chosen such that the corresponding Gram matrix is

as close as possible to the identity Bai et al., 2015, i.e.,

$$\mathbf{G} = \mathbf{\Psi}^T \mathbf{\Phi}^T \mathbf{\Phi} \mathbf{\Psi} \approx \mathbf{I}. \tag{2.3}$$

Note that if the dictionary $\mathbf{\Psi}$ is an orthogonal basis ($\mathbf{\Psi}^T \mathbf{\Psi} = \mathbf{I}$), in order to have (2.3), it make sense to choose $\mathbf{\Phi}$ such that $\mathbf{\Phi}^T \mathbf{\Phi} \approx \mathbf{I}$. Thus, the design of the sensing matrix reduces to an appropriate choice of $\mathbf{\Phi}$. We propose to choose the matrix $\mathbf{\Phi}$ as a binary matrix containing only one 1 per column, in order to reduce the off-diagonal elements of $\mathbf{\Phi^T \Phi}$. Denote as $\boldsymbol{c} = [c_0, \cdots, c_{N_H-1}]^T$ the vector such that

$$c_j = \sum_{i=0}^{P-1} \Phi_{H_{i,j}} + \sum_{i=0}^{Q-1} \Phi_{M_{i,j}} \tag{2.4}$$

where c_j corresponds to the number of ones in the jth column of $\mathbf{\Phi}$, for $j = 0, ..., N_H - 1$, $N_H = MNL$ is the number of columns of the matrix Φ, $\Phi_{H_{i,j}}$ and $\Phi_{M_{i,j}}$ are the elements of the ith row and jth column of the sensing matrices $\mathbf{\Phi}_H$ and $\mathbf{\Phi}_M$, respectively. When each column of Φ contains exactly one 1 and all other values are 0, the matrix Φ satisfies the following relations

$$\sigma_c^2 = \frac{1}{N_H} \sum_{j=0}^{N_H-1} (c_j - \overline{c})^2 = 0, \quad \overline{c} = 1. \tag{2.5}$$

Since these conditions are too restrictive in practice, we propose to design the matrix $\mathbf{\Phi}$ by minimizing the variance σ_c^2 with the constraint $\overline{c} = 1$. Since the entries of $\boldsymbol{c}$ are binary, this problem can be solved using the direct binary search algorithm (see Cuadros et al., 2015 for more details).

3. FUSING CS IMAGES USING A REGULARIZED INVERSE PROBLEM

3.1. INTRODUCTION

The fusion strategy adopted in this work is based on the inverse problem (mentioned before)

$$\widehat{\mathbf{f}} = \arg\ \min_{\mathbf{f}} \frac{1}{2}||\mathbf{\Phi}_H\mathbf{f} - \mathbf{y}_H||_2^2 + \frac{1}{2}||\mathbf{\Phi}_M\mathbf{f} - \mathbf{y}_M||_2^2 + \phi(\mathbf{f}) \tag{3.1}$$

where the two first terms are the data fidelity terms associated with the HS and MS observations and the last term ensures an appropriate regularization. The unknown image is then estimated as $\widehat{\mathbf{f}} = \mathbf{\Psi}\widehat{\mathbf{x}}$. We remind here that $\mathbf{\Psi} \in \mathbb{R}^{N_H \times N_H}$ is a basis in which the image has a sparse representation, that $\mathbf{x} \in \mathbb{R}^{N_H}$ contains the coefficients of $\mathbf{f}$ on this basis, and that $||\cdot||_2$ is the l_2 norm, which is widely used for this kind of inverse problem. The regularization term considered in this work is

$$\phi(\mathbf{f}) = \lambda_1||\mathbf{\Psi}^T\mathbf{f}||_1 + \lambda_2||\boldsymbol{\mathcal{L}}\mathbf{f}||_1 \tag{3.2}$$

which attempts to preserve the sparsity of the coefficients $\mathbf{x} = \mathbf{\Psi}^T\mathbf{f}$ in the domain of the representation basis $\mathbf{\Psi}$, and the smoothness of $\mathbf{f}$ in the spatial domain by using the operator $\boldsymbol{\mathcal{L}}$, which enforce piecewise constant solutions, and is associated with the TV regularizer (see Bras et al., 2012 for more details). Note that $||\cdot||_1$ is the l_1 norm, repectively, and λ_1, λ_2 are regularization parameters Afonso, Bioucas-Dias, and Figueiredo, 2011.

3.2. **PROPOSED ADMM**

The direct solution of problem (3.1) involves the inversion of large matrices, which carries high computational costs. To decouple the original problem in small pieces, let us decouple also

$$\begin{aligned}
\boldsymbol{\Phi}_H &= \begin{bmatrix} \boldsymbol{\Phi}_{H,1}, & \cdots, & \boldsymbol{\Phi}_{H,K} \end{bmatrix}, \\
\boldsymbol{\Phi}_M &= \begin{bmatrix} \boldsymbol{\Phi}_{M,1}, & \cdots, & \boldsymbol{\Phi}_{M,K} \end{bmatrix}, \\
\mathbf{y} &= \begin{bmatrix} \mathbf{y}_H \\ \mathbf{y}_M \end{bmatrix} = \begin{bmatrix} \mathbf{y}_1 \\ \vdots \\ \mathbf{y}_K \\ - \\ \mathbf{y}_{K+1} \\ \vdots \\ \mathbf{y}_{2K} \end{bmatrix},
\end{aligned} \tag{3.3}$$

in order to obtain $2K$ simple problems with respect to (w.r.t.) $\mathbf{f}$. An alternative way to solve (3.1) with the regularizer (3.2) is to split the objective function such as

$$\begin{aligned}
&\underset{\boldsymbol{\nu}_s, \boldsymbol{u}}{\text{minimize}}\ f(\boldsymbol{\nu}_s, \boldsymbol{u}) \\
&\text{subject to } \mathbf{f} = \boldsymbol{\nu}_s; s = 1, \ldots, 2K \\
&\mathbf{f} = \boldsymbol{\Psi} \boldsymbol{u}_2 \\
&\boldsymbol{u}_4 = \boldsymbol{\mathcal{L}} \mathbf{f}
\end{aligned} \tag{3.4}$$

where

$$
\begin{aligned}
f(\boldsymbol{\nu}_s, \boldsymbol{u}) = & \frac{1}{2} \sum_{s=1}^{K} \|\boldsymbol{\Phi}_{H,s} \boldsymbol{\nu}_s - \mathbf{y}_s\|_2^2 + \\
& \frac{1}{2} \sum_{s=1}^{K} \|\boldsymbol{\Phi}_{M,s} \boldsymbol{\nu}_{K+s} - \mathbf{y}_{K+s}\|_2^2 + \phi_2(\boldsymbol{u})
\end{aligned}
\tag{3.5}
$$

where the summations in the two first terms are also related to a splitting of the matrices $\boldsymbol{\Phi}_H$ and $\boldsymbol{\Phi}_M$ into the matrices associated with each snapshot. Then the procedure consists of optimizing the objective function $f(\boldsymbol{\nu}_s, \boldsymbol{u})$ w.r.t. $\boldsymbol{\nu}_s$ and $\boldsymbol{u}$, which leads to Algorithm 1.

Algorithm 1 ADMM Compressive spectral image fusion

1: **Input** $\boldsymbol{\Phi}_H$, $\boldsymbol{\Phi}_M$, $\mathbf{y}$
2: **Initialization** ($\boldsymbol{\nu}$, $\boldsymbol{u}$, $\mathbf{f}$) $= 0$
3: **repeat**
   % Optimize w.r.t $\boldsymbol{\nu}_s$ (see Algorithm 2)
4: $\quad \boldsymbol{\nu}_s^{\ell} = \underset{\boldsymbol{\nu}_s}{\text{minimize}}\ f(\boldsymbol{\nu}_s, \boldsymbol{u}^{\ell-1})$
   % Optimize w.r.t $\boldsymbol{u}$ (see Algorithm 3)
5: $\quad \boldsymbol{u}^{\ell} = \underset{\boldsymbol{u}}{\text{minimize}}\ f(\boldsymbol{\nu}_s^{\ell}, \boldsymbol{u})$
   % Estimate $\mathbf{f}$ (see equation (3.18))
6: $\quad \mathbf{f}^{\ell} \leftarrow$ solve (3.4) w.r.t. $\mathbf{f}$
7: **until** some stopping criterion is satisfied
8: **return** $\mathbf{f}^{\ell}$

An approach for solving (3.4) is to minimize its augmented Lagrangian, which follows from the Alternating Direction Method of Multipliers (ADMM) principles Boyd et al., 2011. ADMM is an algorithm that is intended to blend the decomposability of dual ascent with the superior convergence properties of the method of multipliers. A simple but powerful algorithm that is well suited to distributed convex optimization. It takes the form of a decomposition-coordination procedure, in which the solutions to small local subproblems are coordinated to find a solution to a large global problem. ADMM can be viewed as an attempt to blend the benefits of dual decomposition and

augmented Lagrangian methods for constrained optimization, which can be competitive with the best known methods for some problems Boyd et al., 2011. The Lagrangian for our problem and its optimization will be defined by pieces in the next subsections.

3.2.1. **Optimization w.r.t.** $\boldsymbol{\nu}_s$: Let us express the set of $\boldsymbol{\nu}$ as

$$\begin{bmatrix} \boldsymbol{\nu}_H \\ \boldsymbol{\nu}_M \end{bmatrix} = \begin{bmatrix} \boldsymbol{\nu}_1 \\ \vdots \\ \boldsymbol{\nu}_K \\ - \\ \boldsymbol{\nu}_{K+1} \\ \vdots \\ \boldsymbol{\nu}_{2K} \end{bmatrix}, \tag{3.6}$$

The minimization w.r.t. the variables $\boldsymbol{\nu}_s$ has to be formulated separatelly for every $\boldsymbol{\nu}_H$ and $\boldsymbol{\nu}_M$, for instance, the minimization of the Lagrangian of (3.5) w.r.t. $\boldsymbol{\nu}_H$ can be formulate as

$$\underset{\boldsymbol{\nu}_H}{\text{minimize}}\ L(\boldsymbol{\nu}_H), \tag{3.7}$$

where

$$\begin{aligned} L(\boldsymbol{\nu}_H) =& \frac{1}{2}\sum_{s=1}^{K} \|\boldsymbol{\Phi}_{M,s}\boldsymbol{\nu}_s - \mathbf{y}_s\|_2^2 + \\ & \frac{\rho}{2}\sum_{s=1}^{K} \|\mathbf{f} - \boldsymbol{\nu}_s + \mathbf{d}_s\|_2^2 \end{aligned} \tag{3.8}$$

where $\mathbf{d}_s$ is a slack variable, the update term for $\boldsymbol{\nu}_H$ can be obtained by differentiating (3.8) w.r.t. $\boldsymbol{\nu}_H$ and forcing it to be zero. Note that the Lagrangian of $\boldsymbol{\nu}_M$ can be derived from the lagrangian of $\boldsymbol{\nu}_H$, by repleazing $\boldsymbol{\Phi}_H$ by $\boldsymbol{\Phi}_M$, $\boldsymbol{\nu}_M$ by $\boldsymbol{\nu}_H$, and $\mathbf{y}_M$ by $\mathbf{y}_H$. Algorithm 2 shows how $\boldsymbol{\nu}_H$ and $\boldsymbol{\nu}_M$ are updated from the minimization of their respectives Lagrangians. Notice that $\mathbb{I}_{N_H}$ is the identity matrix of size $N_H \times N_H$

Algorithm 2

1: **Input** $\boldsymbol{\Phi}_H$, $\boldsymbol{\Phi}_M$, $\mathbf{y}$
2: **Initialization** ($\boldsymbol{\nu}_H$, $\boldsymbol{\nu}_M$, $\mathbf{d}$, $\mathbf{f}$) $= 0$
3: **repeat**
   % updating $\boldsymbol{\nu}_H$
4: $\boldsymbol{\nu}_H^{\ell} = \sum_{s=1}^{K} \left(\left(\boldsymbol{\Phi}_{H,s}^T \boldsymbol{\Phi}_{H,s} \right) + \rho \mathbb{I}_{N_H} \right)^{-1} \left(\rho \left(\mathbf{f}^{\ell-1} + \mathbf{d}_s^{\ell} \right) + \boldsymbol{\Phi}_{H,s}^T \mathbf{y}_s \right)$
   % updating $\boldsymbol{\nu}_M$
5: $\boldsymbol{\nu}_M^{\ell} = \sum_{s=1}^{K} \left(\left(\boldsymbol{\Phi}_{M,s}^T \boldsymbol{\Phi}_{M,s} \right) + \rho \mathbb{I}_{N_H} \right)^{-1} \left(\rho \left(\mathbf{f}^{\ell-1} + \mathbf{d}_{K+s}^{\ell} \right) + \boldsymbol{\Phi}_{M,s}^T \mathbf{y}_{K+s} \right)$
6: **until** some stopping criterion is satisfied
7: **return** $\boldsymbol{\nu}_H^{\ell}$, $\boldsymbol{\nu}_M^{\ell}$

and that the sparsity of the matrices $\boldsymbol{\Phi}_H$ and $\boldsymbol{\Phi}_M$ allows the matrices $(\boldsymbol{\Phi}_{H,s}^T \boldsymbol{\Phi}_{H,s} + \rho \mathbb{I}_{N_H}) \in \mathbb{R}^{N_H \times N_H}$ and $(\boldsymbol{\Phi}_{M,s}^T \boldsymbol{\Phi}_{M,s} + \rho \mathbb{I}_{N_H}) \in \mathbb{R}^{N_H \times N_H}$ to be inverted with reasonable computational complexity.

3.2.2. **Optimization w.r.t. $\boldsymbol{u}$** : Let us remind that the problem (3.1) has became

$$\begin{aligned} &\underset{\boldsymbol{\nu}, \boldsymbol{u}}{\text{minimize}} \; L(\boldsymbol{\nu}_H) + L(\boldsymbol{\nu}_M) + \lambda_1 ||\boldsymbol{u}_2||_1 + \lambda_2 ||\boldsymbol{u}_4||_1 \\ &\text{subject to } \mathbf{f} = \boldsymbol{\Psi} \boldsymbol{u}_2. \\ &\qquad\qquad \boldsymbol{u}_4 = \boldsymbol{\mathcal{L}} \mathbf{f}. \end{aligned} \tag{3.9}$$

This minimization w.r.t. $\boldsymbol{u}$ can be solved by introducing auxiliary variables to split the regularization term. More specifically, by introducing the splitting, $\boldsymbol{u}_2 = \boldsymbol{u}_1$ and

$\boldsymbol{u}_4 = \boldsymbol{u}_3$, the problem (3.9) becomes

$$\begin{aligned} &\underset{\boldsymbol{v}_s, \boldsymbol{u}}{\text{minimize}}\ L(\boldsymbol{\nu}_H) + L(\boldsymbol{\nu}_M) + \lambda_1 \left\|\boldsymbol{u}_1\right\|_1 + \lambda_2 \left\|\boldsymbol{u}_3\right\|_{TV} \\ &\text{subject to } \mathbf{f} = \boldsymbol{\Psi}\boldsymbol{u}_2. \\ &\qquad\qquad \boldsymbol{u}_2 = \boldsymbol{u}_1. \\ &\qquad\qquad \boldsymbol{u}_4 = \boldsymbol{\mathcal{L}}\mathbf{f}. \\ &\qquad\qquad \boldsymbol{u}_4 = \boldsymbol{u}_3. \end{aligned} \tag{3.10}$$

For solving the problem (3.10) we have to optimize the Lagrangian of every $\boldsymbol{u}$, for instance, the optimization w.r.t. $\boldsymbol{u}_1$ can be formulated as

$$\underset{\boldsymbol{u}_1}{\text{minimize}}\ L(\boldsymbol{u}_1), \tag{3.11}$$

where

$$L(\boldsymbol{u}_1) = \lambda_1 \left\|\boldsymbol{u}_1\right\|_1 + \frac{\rho}{2}\left\|\boldsymbol{u}_2 - \boldsymbol{u}_1 + \mathbf{d}_{(2K+1)}\right\|_2^2, \tag{3.12}$$

and the optimization w.r.t. $\boldsymbol{u}_2$ can be formulated as

$$\underset{\boldsymbol{u}_2}{\text{minimize}}\ L(\boldsymbol{u}_2), \tag{3.13}$$

where

$$\begin{aligned} L(\boldsymbol{u}_2) = &\frac{\rho}{2}\left\|\boldsymbol{u}_2 - \boldsymbol{u}_1 + \mathbf{d}_{(2K+1)}\right\|_2^2 + \\ &\frac{\rho}{2}\left\|\mathbf{f} - \boldsymbol{\Psi}\boldsymbol{u}_2 + \mathbf{d}_{(2K+2)}\right\|_2^2 \end{aligned} \tag{3.14}$$

where the variables $\mathbf{d}$ also are slack variables. The optimization w.r.t. $\boldsymbol{u}_3$ and $\boldsymbol{u}_4$ can be derived from $\boldsymbol{u}_1$ and $\boldsymbol{u}_2$ by replacing the variables. The update terms for each $\boldsymbol{u}$ can be found by differentiating the Lagrangians and forcing it to be zero. However,

$L(\boldsymbol{u}_1)$ and $L(\boldsymbol{u}_3)$ are not differentiable, we update these parameters using the soft thresholding operations which result from the computation of appropriate proximal operators (see Boyd et al., 2011; Bras et al., 2012 for details). Algorithm 3 shows how each $\boldsymbol{u}$ is updated from the minimization of their respective Lagrangians

Algorithm 3

Input $\boldsymbol{\Psi}_H$, $\boldsymbol{\mathcal{L}}$
Initialization $(\boldsymbol{u}, \mathbf{d}, \mathbf{f}) = 0$
repeat
  % updating $\boldsymbol{u}_1$
    $\boldsymbol{u}_1^{\ell} = S_{\lambda_1/\rho}(\boldsymbol{u}_2^{\ell-1} + \mathbf{d}_{2K+1}^{\ell-1})$
  % updating $\boldsymbol{u}_2$
    $\boldsymbol{u}_2^{\ell} = \left(\left(\boldsymbol{\Psi}^T\boldsymbol{\Psi}\right) + \mathbb{I}_{N_H}\right)^{-1}$
      $\left(\boldsymbol{\Psi}\left(\mathbf{f}^{\ell-1} + \mathbf{d}_{(2K+2)}^{\ell-1}\right) + \boldsymbol{u}_1^{\ell} + \mathbf{d}_{(2K+1)}^{\ell-1}\right)$
  % updating $\boldsymbol{u}_3$
    $\boldsymbol{u}_3^{\ell} = S_{\lambda_2/\rho}(\boldsymbol{u}_4^{\ell-1} + \mathbf{d}_{2K+3}^{\ell-1}))$
  % updating $\boldsymbol{u}_4$
    $\boldsymbol{u}_4^{\ell} = \left(\left(\boldsymbol{\mathcal{L}}^T\boldsymbol{\mathcal{L}}\right) + \mathbb{I}_{N_H}\right)^{-1}$
      $\left(\boldsymbol{\mathcal{L}}\left(\mathbf{f}^{\ell-1} + \mathbf{d}_{(2K+4)}^{\ell-1}\right) + \boldsymbol{u}_3^{\ell} + \mathbf{d}_{(2K+3)}^{\ell-1}\right)$
until some stopping criterion is satisfied
return $\boldsymbol{u}^{\ell}$

where

$$S_{\lambda_1/\rho} = \begin{cases} \boldsymbol{u}_2 + \mathbf{d}_{2K+1} - \frac{\lambda_1}{\rho} & \text{if } \boldsymbol{u}_2 + \mathbf{d}_{2K+1} > \frac{\lambda_1}{\rho} \\ \boldsymbol{u}_2 + \mathbf{d}_{2K+1} + \frac{\lambda_1}{\rho} & \text{if } \boldsymbol{u}_2 + \mathbf{d}_{2K+1} < -\frac{\lambda_1}{\rho} \\ 0 & \text{otherwise} \end{cases} \tag{3.15}$$

and

$$S_{\lambda_2/\rho} = \begin{cases} \boldsymbol{u}_4 + \mathbf{d}_{2K+3} - \frac{\lambda_2}{\rho} & \text{if } \boldsymbol{u}_4 + \mathbf{d}_{2K+3} > \frac{\lambda_2}{\rho} \\ \boldsymbol{u}_4 + \mathbf{d}_{2K+3} + \frac{\lambda_2}{\rho} & \text{if } \boldsymbol{u}_4 + \mathbf{d}_{2K+3} < -\frac{\lambda_2}{\rho} \\ 0 & \text{otherwise} \end{cases} \tag{3.16}$$

3.2.3. **Estimating** $\mathbf{f}$: Finally, we are able to estimate the unknown image $\mathbf{f}$ from (3.10) by minimizing its Lagrangian w.r.t. $\mathbf{f}$, which can be defined as

$$\begin{aligned} L(\mathbf{f}) =& \frac{\rho}{2}\Big(\sum_{s=1}^{K} \|\mathbf{f} - \boldsymbol{\nu}_s + \mathbf{d}_s\|_2^2 + \sum_{s=1}^{K} \|\mathbf{f} - \boldsymbol{\nu}_{K+s} + \mathbf{d}_{K+s}\|_2^2 \\ & \left\|\mathbf{f} - \boldsymbol{\Psi}\boldsymbol{u}_2 + \mathbf{d}_{(2K+2)}\right\|_2^2 + \left\|\mathbf{f} - \boldsymbol{\mathcal{L}}\boldsymbol{u}_4 + \mathbf{d}_{(2K+4)}\right\|_2^2 \Big). \end{aligned} \tag{3.17}$$

Notice that every term comes from $L(\boldsymbol{\nu}_H)$, $L(\boldsymbol{\nu}_M)$, $L(\boldsymbol{u}_2)$ and $L(\boldsymbol{u}_4)$, respectively. The optimization of $L(\mathbf{f})$ can be perform by differentiating and forcing it to be zero, which results in

$$\begin{aligned} \mathbf{f} =& \frac{1}{4}\Bigg(\sum_{s=1}^{2K} (\boldsymbol{\nu}_s - \mathbf{d}_s) + \\ & \left(\boldsymbol{\Psi}\boldsymbol{u}_2 - \mathbf{d}^{\ell}_{(2K+2)}\right) + \left(\boldsymbol{u}_{(3)} - \mathbf{d}^{\ell}_{(2K+4)}\right) \Bigg) \end{aligned} \tag{3.18}$$

which corresponds to the update term for $\mathbf{f}$ in line 5 of the algorithm 1.

3.3. **CONVERGENCE**

Note that we start from the convex relaxation of the CS problem. Due to the functions f and ϕ are convex, we have the implication that the subproblems arising in the update of each variable are solvable, i.e., there exist f, not necessarily unique, that minimize the augmented Lagrangian.

4. SIMULATIONS AND RESULTS

4.1. INTRODUCTION

Two imagers were considered to generate the low spatial/high spectral and high spatial/low spectral resolution measurements $\mathbf{y}_H$ and $\mathbf{y}_M$ in every experiment. Both systems used the same high-resolution image, which was compressed by two ways, using spatial and spectral degradations, respectively. The matrix $\mathbf{\Phi}$ was designed using the method described in Chapter 2. The reference image considered in this work is mainly the classical ROSIS image acquired over Pavia, northern Italy Kunkel et al., 1991 reduced to 256×256 pixels and 92 bands. The HS data cube was obtained by applying a 5×5 Gaussian lowpass filter in each band and by using a 4:1 decimation ratio ($p = 2$). Similarly, the MS data was generated by using a 4:1 decimation ratio ($q = 4$). Algorithm 1 was then used to estimate the image $\mathbf{f}$. The main parameters were established as follow:

- The value of λ_1 was selected by cross-validation and we found that the value 5e-4 provides good results for the estimated image.
- The value of λ_2 was selected to be equal to λ_1.
- The parameter ρ was initialized near to zero and was updated as will be depicted in Section 4.2 as suggested in Boyd et al., 2011.
- The dictionary $\mathbf{\Psi}$ was selected as the Kronecker product $\mathbf{W} \otimes \mathbf{T}$, between $\mathbf{W}$, a Symlet Wavelet kernel, and $\mathbf{T}$, a DCT operator, which have been addressed before and exhibits a good performance in spectral image representation Arguello and Arce, 2014.

- The operator $\mathcal{L}$ was decoupled in two operators acting over the rows and over the columns of each spectral band, such as is shown in Barbero and Sra, 2014 for Two-dimensional TV.

- The stopping criterion was selected as is suggested in Boyd et al., 2011. Thus, we establish tolerances for $||\mathbf{f}^{\ell} - \boldsymbol{\nu}^{\ell}||_2 \leq \epsilon_1$ and $||\boldsymbol{\nu}^{\ell-1} - \boldsymbol{\nu}^{\ell}||_2 \leq \epsilon_2$ such that $10^{-2} \leq \epsilon_1, \epsilon_2 \leq 10^{-4}$. However, these are not only our stopping criteria, but also we use 10-30 iterations for each ρ.

4.2. ρ UPDATING

The update of the parameter ρ comes from Boyd et al., 2011 and it works well for a few tens of iterations.

$$\rho^{\ell+1} = \begin{cases} \tau_l \rho^{\ell} & \text{if } ||\mathbf{f}^{\ell} - \boldsymbol{\nu}^{\ell}||_2 > \mu ||\boldsymbol{\nu}^{\ell-1} - \boldsymbol{\nu}^{\ell}||_2 \\ \rho^{\ell} \tau_r & \text{if } ||\boldsymbol{\nu}^{\ell-1} - \boldsymbol{\nu}^{\ell}||_2 > \mu ||\mathbf{f}^{\ell} - \boldsymbol{\nu}^{\ell}||_2 \\ \rho^{\ell} & \text{otherwise} \end{cases} \tag{4.1}$$

where $\tau_l = \tau_r = 2$ $\mu = 10$ are selected by cross validation. In practice, it is inefficient to update ρ for each iteration of the algorithm, for that, the simulations where performed by updating ρ after each 10 iterations of the main algorithm.

4.3. PROPOSED APPROACH AND MATRIX DESIGN TESTING

Several experiments were performed to test the optimization procedure of the Chapter 2, compared with the traditional random matrices. We argue that designed procedure allows to more incoherent measurement matrix to be derived than random

realizations. Fig. 8 Shows the performance of the propossed approach with designed and random measuremnt matrices, for the CASSI, in different compression ratios.

Figure 8: PSNR comparison for the results of the propossed fusion approach, performed by using the CASSI for different compression ratios.

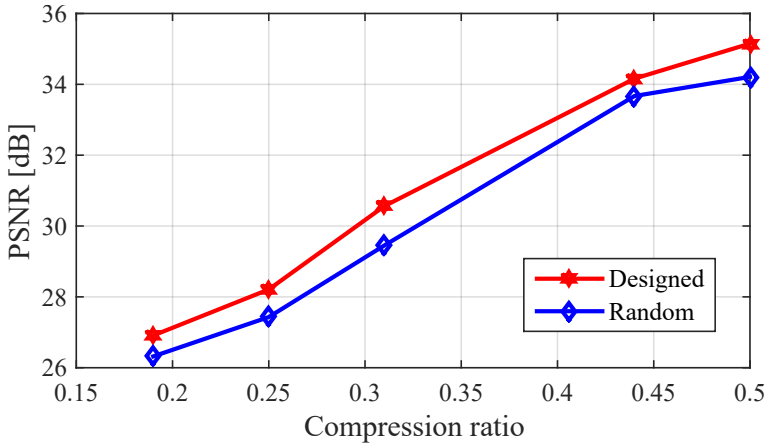

From these results, we can conclude that the designed measurement matrix promotes better results than those with random entries, as expected. By the other side, the SSCSI also was tested in the same simulation scenario, Fig 9 shows the results.

Figure 9: PSNR comparison for the results of the proposed fusion approach, performed by using the SSCSI for different compression ratios.

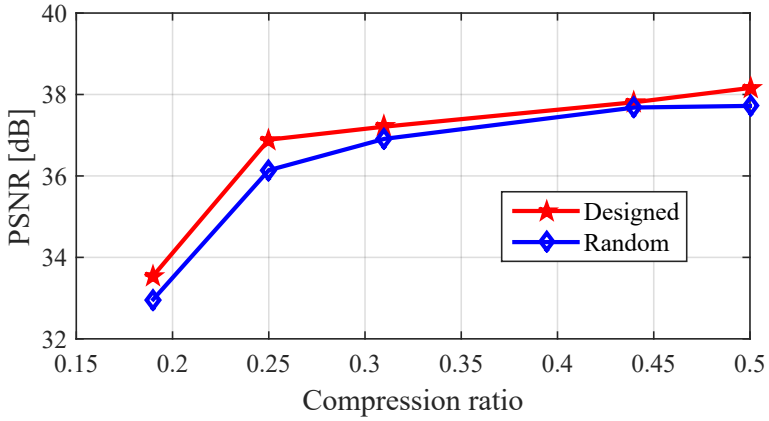

The designing approach show promise results, due to the constrained structure of the matrices used in this work, the optimization procedure is also very constrained

and this proposed here works well. As a theoretical reference, the proposed approach was tested with the Gaussian measurement matrices. The results are presented in Fig. 8, similar to those shown before for the practical systems.

Figure 10: PSNR results of the proposed fusion approach, performed by using the CASSI, SSCSI and Gaussian matrices for different compression ratios

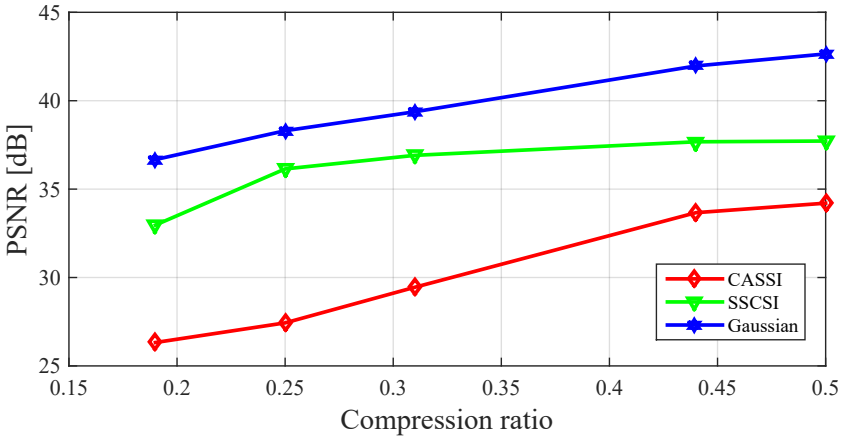

Notice that the results for these matrices are better than those obtained by using other matrices (those from practical systems), as expected. Also that there is a slight difference between the results in Figs. 8 and 9. In general, the results show the superiority of the gaussian coding, with is followed by the spatio-spectral coding, which shows the limitations of the spatial coding. These results make sense with the mutual coherence principle of the CS theory. Finally, a comparison and testing of the proposed approach in the presence of noise was performed, the results are shown in Fig. 11.

Figure 11: PSNR comparison for the results of the proposed fusion approach, performed by using CASSI, SSCSI and Gaussian matrices for different values of SNR on the additive noise

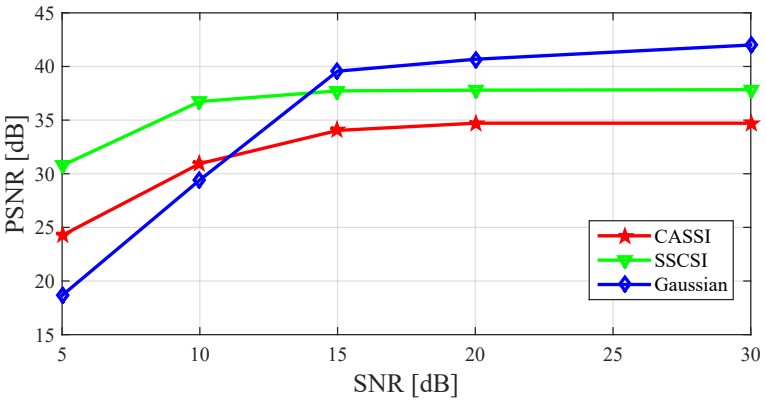

Despite the loss in reconstruction quality, the proposed fusion approach provides a PSNR close to 40 dB for noise with SNR and15 dB, which is very promising. A particular observation from these results are the performance of the different systems in presence of noise, the CASSI and SSCSI systems allow the Gaussian matrix to be overcome in low levels of SNR.

4.4. **SPATIAL AND SPECTRAL RESULTS TESTING**

The simulation results displayed in Figs. 12 and 13 show that the proposed fusion method (at compression ratio of 0.4) provides a reconstructed image close to the reference image in both, spatial and spectral, resolutions. First, Fig. 12 shows visual results of the spatial content of the reconstructions compared with the reference image, these images are from the selection of the red, green and blue bands of the spectral datacubes.

Figure 12: Spatial fusion results for the Pavia dataset. (Top-left) Groundtruht. (Top-right) CASSI Reconstruction of the proposed fusion method (PSRN=30 dB). (Bottom-left) SSCSI Reconstruction of the proposed fusion method (PSNR=38 dB). (Bottom-right) GAUSSIAN Reconstruction of the proposed fusion method (PSNR=41 dB).

On the oher hand, some spectral signatures of particular pixels displayed in Figs. 13 and 14. these selection of pixels comes from a random realization, and it is present the spectral signatures for the fisrt 16 spectral bands. Fig. 13 present a comparison between the spectral signatures obtained from the datacubes reconstructed by using the CASSI, SSCSI and Gaussian matrices, for the pixel $\#(41, 110)$.

Figure 13: Spectral fusion results for the Pavia dataset. Spectral signature of pixel $\#(41, 110)$.

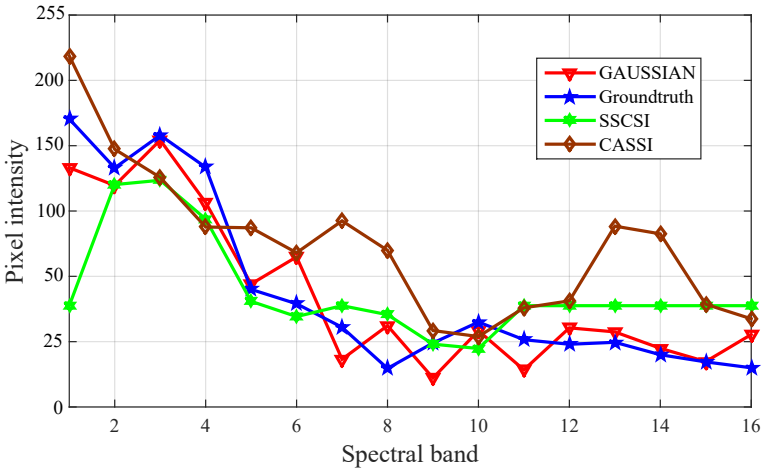

Also, specific results for each matrix are displayed in Fig. 14.

Figure 14: Spectral fusion results. (Top) Spectral signature of pixel $\#(2, 218)$. (Middle) Spectral signature of pixel $\#(185, 43)$. (Bottom) Spectral signature of pixel $\#(13, 230)$.

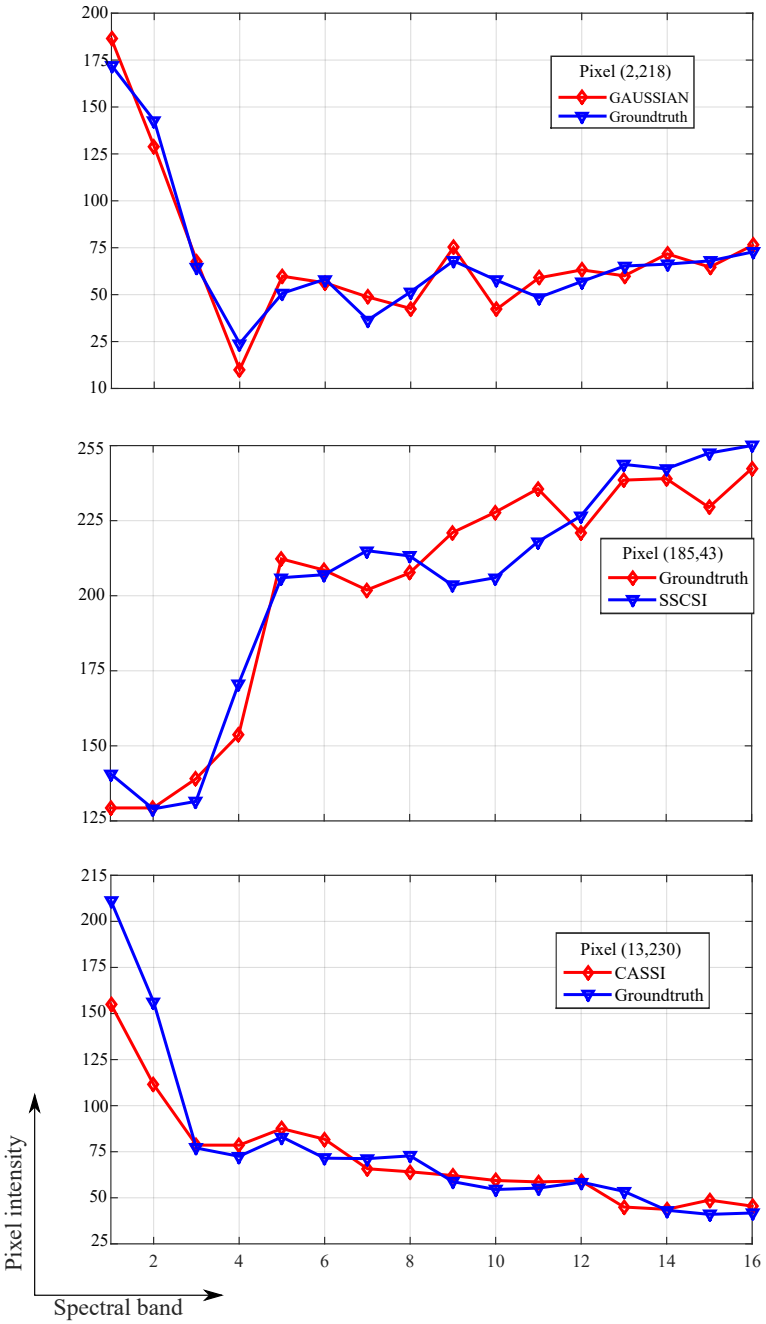

In general, the obtained results are close to the reference and the spatial/spectral resolution of the estimated image is satisfactory.

4.5. **COMPUTATIONAL COMPLEXITY ANALYSIS**

In terms of computational complexity, the number of operations per iteration in Algorithm 1 depends on the underlying signal size and the size of the measurement vector. In particular, the computational complexity the algorithm 2 is proportional to the nonzero elements of the matrix $(\mathbf{\Phi}_{\cdot}^{T}\mathbf{\Phi}_{\cdot}) + \rho\mathbb{I}_{N_H}$. As this term is sparse much more efficient factorization and backsolve routines can be employed (e.g. Cholesky factorization Green et al., 1998; Boyd et al., 2011), then, in this case, these update can be carried out at a cost $O(nk^2)$, plus the cost of forming the term $(\mathbf{\Phi}_{\cdot}^{T}\mathbf{\Phi}_{\cdot}) + \rho\mathbb{I}_{N_H}$. It is also known that those operations in the algorithm 3 can be done in O(N_H). however, it is also necessary to have into account that the inversions have to compute each time as ρ is updated.

4.6. **COMPARISON WITH OTHER METHODS**

Before was mentioned a related fusion method, known as 'Sparse fusion', which exploits the low dimensionality of the spectral images in a sparse domain, for fusing spatiospectral information. A comparison of the Sparse fusion and the proposed fusion approaches is depicted in this subsection. The simulation scenario was established as in the paper Wei et al., 2015. Notice that we only compare the results in term of the spatial (Fig. 15) and spectral (Fig. 16) results and time-consuming (Table 1), because the approaches are no strictly related. Notice also that the Sparse fusion was compared before with another fusion approaches and exhibits good performance.

Table 1: Comparison between Sparse fusion and the proposed approach

	Sparse Fusion	CS Fusion
PSNR	37,51	35,98
Time	10,85	15,49

Figure 15: Spatial fusion results. (Left) Reference image. (Middle) Sparse Fusion result. (Right) Propossed fusion approach (Compression ratio of 0.5).

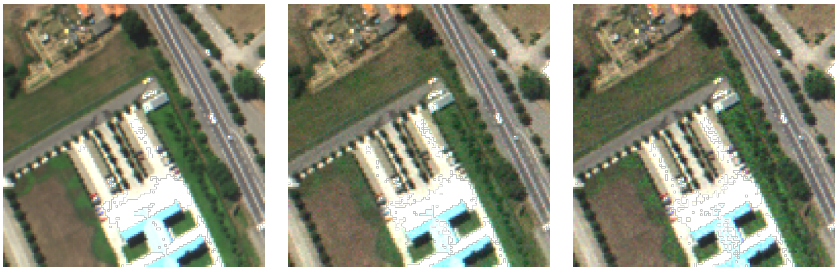

Figure 16: Spectral fusion results. Spectral signature of pixel $\#(36, 89)$.

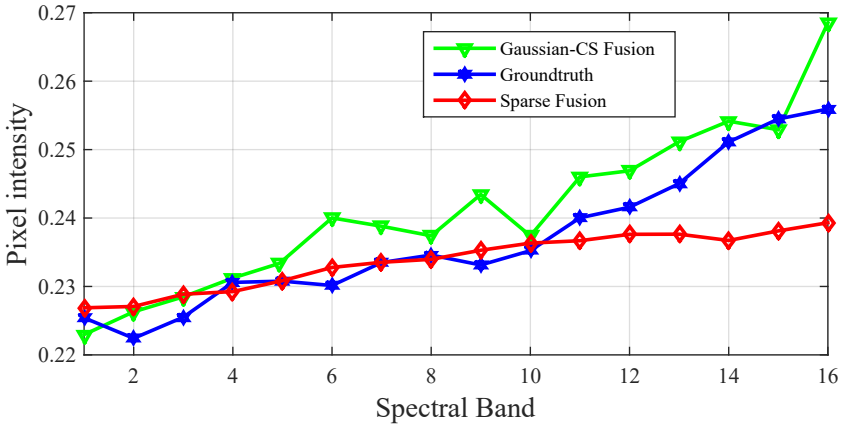

These results show that the propossed approach is comparable to other methods, despite of uses fewer data.

4.7. **TEST WITH ANOTHER DATASET**

The proposed fusion method has been tested with another dataset. Those results are the same presented in subsection 4.4, but with the reference image is the high

spatio-spectral image acquired over Moffett Field, CA, in 2009 by the JPL/NASA airborne visible/infrared imaging spectrometer (AVIRIS) Green et al., 1998.This image was reduced to 256×256 pixels and 128 bands. Fig. 17 shows visual results for the Moffet field dataset, with similar performance to the results for the Pavia dataset.

Figure 17: Spatial fusion results for the Moffett Field dataset. (Top-left) Groundtruht. (Top-right) CASSI Reconstruction of the proposed fusion method (PSRN=30 dB). (Bottom-left) SSCSI Reconstruction of the proposed fusion method (PSNR=37 dB). (Bottom-right) GAUSSIAN Reconstruction of the proposed fusion method (PSNR=42 dB).

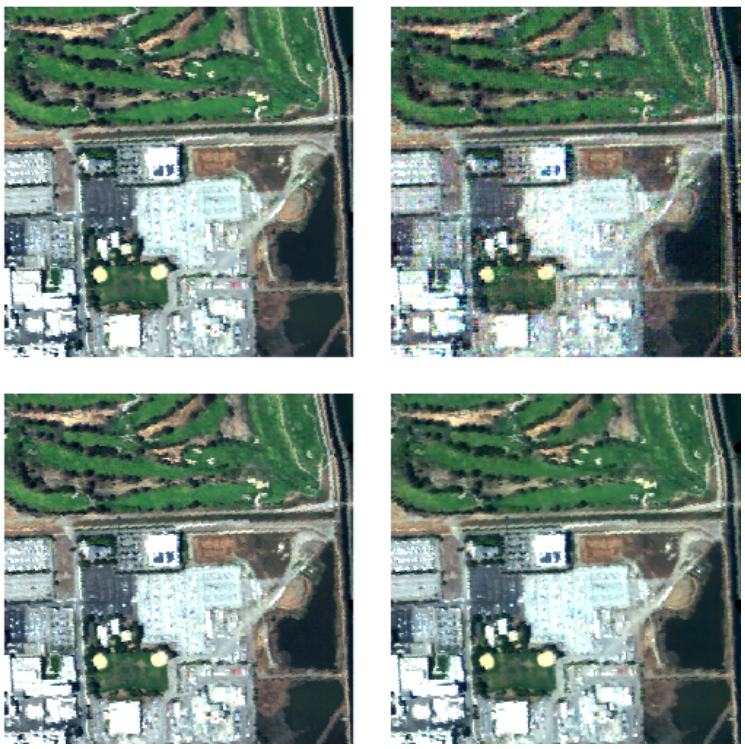

Also, the results in the spectral dimension are presented in Fig. 18.

Figure 18: Spectral fusion results. Spectral signature of pixel $\#(80, 89)$.

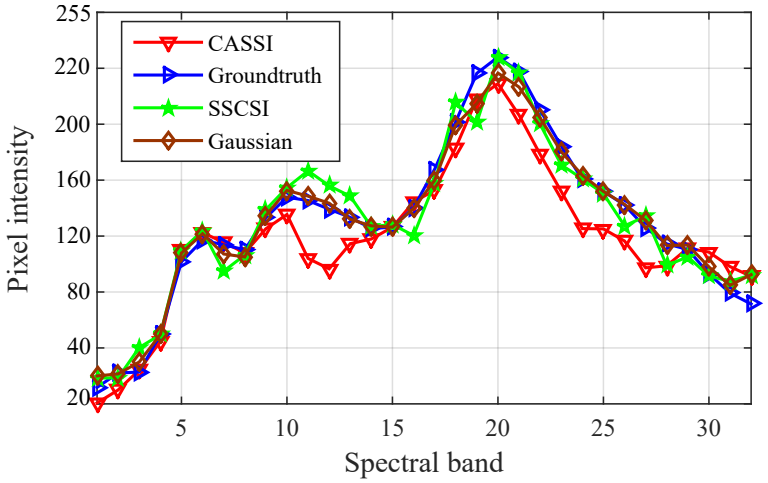

Notice that the results are satisfactory for different datasets in both spatial and spectral resolutions, and also that Gaussian matrices allows the better results for the fusion approach.

5. **CONCLUSIONS**

This work showed that compressive projections can be used to fuse high spectral/low spatial and high spatial/low spectral resolution images without the need of expensive image reconstruction. Our experiments showed that compressive sensing-based algorithms can be used to reconstruct images with high spatial and spectral resolutions using as few as 50% of data acquired by multiple sensors. In this work, the simulations obtained from a CS operation yielded reconstructed images with PSNRs larger than 35dB, which is comparable with those obtained with other fusion approaches, even in the presence of noise. The advantage of the proposed fusion rule is the reduced cost of the acquisition system and the reduced computational complexity of the reconstruction method.

6. BIBLIOGRAPHIC REFERENCES

[1] M. V. Afonso, J. M. Bioucas-Dias, and M. A. T. Figueiredo, "An augmented lagrangian approach to the constrained optimization formulation of imaging inverse problems", *IEEE Trans. Image Process.*, vol. 20, no. 3, Mar. 2011. arXiv: 0912.3481 [math.OC].

[2] G. R. Arce, D. J. Brady, L. Carin, H. Arguello, and D. S. Kittle, "Compressive coded aperture spectral imaging: An introduction", *IEEE Signal Process. Mag.*, vol. 31, no. 1, pp. 105–115, 2014, ISSN: 1053-5888. DOI: 10.1109/MSP.2013.2278763.

[3] H. Arguello and G. R. Arce, "Colored coded aperture design by concentration of measure in compressive spectral imaging", *IEEE Trans. Image Process.*, vol. 23, no. 4, pp. 1896–1908, 2014, ISSN: 1057-7149. DOI: 10.1109/TIP.2014.2310125.

[4] H. Bai, G. Li, S. Li, Q. Li, Q. Jiang, and L. Chang, "Alternating optimization of sensing matrix and sparsifying dictionary for compressed sensing", *IEEE Transactions on Signal Processing*, vol. 63, no. 6, pp. 1581–1594, 2015, ISSN: 1053-587X. DOI: 10.1109/TSP.2015.2399864.

[5] Á. Barbero and S. Sra, "Modular proximal optimization for multidimensional total-variation regularization", *ArXiv e-prints*, Nov. 2014. arXiv: 1411.0589 [stat.ML].

[6] G. Bellante, S. Powell, R. Lawrence, K. Repasky, and T. Dougher, "Aerial detection of a simulated co2 leak from a geologic sequestration site using hyperspectral imagery", *International Journal of Greenhouse Gas Control*, vol. 13,

pp. 124–137, 2013, ISSN: 17505836. DOI: 10.1016/j.ijggc.2012.11.034.

[7] J. M Bioucas-Dias, A. Plaza, G. Camps-valls, P. Scheunders, N. Nasrabadi, and J. Chanussot, "Hyperspectral remote sensing data analysis and future challenges", *IEEE Geosci. Remote Sens. Mag.*, vol. 1, no. 2, pp. 6–36, 2013, ISSN: 2168-6831.

[8] S. Boyd, N. Parikh, E. Chu, B. Peleato, and J. Eckstein, "Distributed optimization and statistical learning via the alternating direction method of multipliers", *Found. Trends Mach. Learn.*, vol. 3, no. 1, pp. 1–122, Jan. 2011, ISSN: 1935-8237. DOI: 10.1561/2200000016.

[9] N. B. Bras, J. Bioucas-Dias, R. C. Martins, and A. C. Serra, "An alternating direction algorithm for total variation reconstruction of distributed parameters", *IEEE Transactions on Image Processing*, vol. 21, no. 6, pp. 3004–3016, 2012, ISSN: 1057-7149. DOI: 10.1109/TIP.2012.2188033.

[10] E. J. Candes and M. B. Wakin, "An introduction to compressive sampling", *IEEE Signal Process. Mag.*, vol. 25, no. 2, pp. 21–30, 2008, ISSN: 1053-5888. DOI: 10.1109/MSP.2007.914731.

[11] A. P. Cuadros, C. Peitsch, H. Arguello, and G. R. Arce, "Coded aperture optimization for compressive x-ray tomosynthesis", *Opt. Express*, vol. 23, no. 25, pp. 32 788–32 802, 2015. DOI: 10.1364/OE.23.032788.

[12] J. E. Fowler, "Compressive-projection principal component analysis", *IEEE Transactions on Image Processing*, vol. 18, no. 10, pp. 2230–2242, 2009, ISSN: 1057-7149. DOI: 10.1109/TIP.2009.2025089.

[13] R. O. Green, M. L. Eastwood, C. M. Sarture, T. G. Chrien, M. Aronsson, B. J. Chippendale, J. A. Faust, B. E. Pavri, C. J. Chovit, M. Solis, M. R. Olah, and

O. Williams, “Imaging spectroscopy and the airborne visible/infrared imaging spectrometer (aviris)”, *Remote Sensing of Environment*, vol. 65, no. 3, pp. 227 –248, 1998, ISSN: 0034-4257. DOI: http://doi.org/10.1016/S0034-4257(98)00064-9.

[14] B. Kunkel, F. Blechinger, D. Viehmann, H. V. D. Piepen, and R. Doerffer, “Rosis imaging spectrometer and its potential for ocean parameter measurements (airborne and space-borne)”, *Int. J. of Remote Sens.*, vol. 12, no. 4, pp. 753–761, 1991. DOI: 10.1080/01431169108929691.

[15] X. Lin, Y. Liu, J. Wu, and Q. Dai, “Spatial-spectral encoded compressive hyperspectral imaging”, *ACM Trans. Graph.*, vol. 33, no. 6, 233:1–233:11, 2014, ISSN: 0730-0301.

[16] G. Lu and B. Fei, “Medical hyperspectral imaging: a review”, *Journal of biomedical optics*, vol. 19, no. 1, p. 10 901, 2014, ISSN: 1560-2281. DOI: 10.1117/1.JBO.19.1.010901.

[17] X. Luo, J. Zhang, J. Yang, and Q. Dai, “Classification-based image-fusion framework for compressive imaging”, *Journal of Electronic Imaging*, vol. 19, no. 3, pp. 033 009–033009–14, 2010. DOI: 10.1117/1.3478879.

[18] G. Martín, J. M. Bioucas-Dias, and A. Plaza, “Hyca: A new technique for hyperspectral compressive sensing”, *IEEE Transactions on Geoscience and Remote Sensing*, vol. 53, no. 5, pp. 2819–2831, 2015, ISSN: 0196-2892. DOI: 10.1109/TGRS.2014.2365534.

[19] F. Medina, H.Arguello, and C. Gómez, “A quantitative and qualitative performance analysis of compressive spectral imagers”, *Revista Tecnura*, 2017.

[20] D. Needell and R. Ward, “Stable image reconstruction using total variation minimization”, *SIAM Journal on Imaging Sciences*, vol. 6, no. 2, pp. 1035–1058,

2013. DOI: 10.1137/120868281. eprint: http://dx.doi.org/10.1137/120868281.

[21] R. Rubinstein, A. M. Bruckstein, and M. Elad, "Dictionaries for sparse representation modeling", *Proceedings of the IEEE*, vol. 98, no. 6, pp. 1045–1057, 2010, ISSN: 0018-9219. DOI: 10.1109/JPROC.2010.2040551.

[22] J. Ryan, C. Davis, N. Tufillaro, R. Kudela, and B.-C. Gao, "Application of the hyperspectral imager for the coastal ocean to phytoplankton ecology studies in monterey bay, ca, usa", *Remote Sensing*, vol. 6, no. 2, pp. 1007–1025, 2014, ISSN: 2072-4292. DOI: 10.3390/rs6021007.

[23] I. Tosic and P. Frossard, "Dictionary learning", *IEEE Signal Processing Magazine*, vol. 28, no. 2, pp. 27–38, 2011, ISSN: 1053-5888.

[24] A. Wagadarikar, R. John, R. Willett, and D. Brady, "Single disperser design for coded aperture snapshot spectral imaging.", *Appl. Opt.*, vol. 47, no. 10, B44–51, Apr. 2008, ISSN: 0003-6935.

[25] Q. Wei, N. Dobigeon, and J. Y. Tourneret, "Bayesian fusion of multi-band images", *IEEE Journal of Selected Topics in Signal Processing*, vol. 9, no. 6, pp. 1117–1127, 2015, ISSN: 1932-4553. DOI: 10.1109/JSTSP.2015.2407855.

[26] Q. Wei, J. Bioucas-Dias, N. Dobigeon, and J. Y. Tourneret, "Hyperspectral and multispectral image fusion based on a sparse representation", *IEEE Trans. Geosci. Remote Sens.*, vol. 53, no. 7, pp. 3658–3668, 2015, ISSN: 0196-2892.

[27] Q. Wei, S. Godsill, J. M. Bioucas-Dias, N. Dobigeon, and J. Y. Tourneret, "High-resolution hyperspectral image fusion based on spectral unmixing", in *2016 19th International Conference on Information Fusion (FUSION)*, 2016, pp. 1714–1719.

[28] Z. Xiong, A. Xie, D.-W. Sun, X.-A. Zeng, and D. Liu, “Applications of hyperspectral imaging in chicken meat safety and quality detection and evaluation: a review”, *Critical reviews in food science and nutrition*, null, 2014, ISSN: 1549-7852. DOI: 10.1080/10408398.2013.834875.

[29] H. Yin, Z. Liu, B. Fang, and Y. Li, “A novel image fusion approach based on compressive sensing”, *Optics Communications*, vol. 354, pp. 299 –313, 2015, ISSN: 0030-4018. DOI: http://dx.doi.org/10.1016/j.optcom.2015.05.020.

BIBLIOGRAPHY

Afonso, M. V., J. M. Bioucas-Dias, and M. A. T. Figueiredo (2011). "An augmented lagrangian approach to the constrained optimization formulation of imaging inverse problems". In: *IEEE Trans. Image Process.* 20.3. arXiv: 0912.3481 [math.OC].

Arce, G. R. et al. (2014). "Compressive Coded Aperture Spectral Imaging: An Introduction". In: *IEEE Signal Process. Mag.* 31.1, pp. 105–115. ISSN: 1053-5888. DOI: 10.1109/MSP.2013.2278763.

Arguello, H. and G. R. Arce (2014). "Colored Coded Aperture Design by Concentration of Measure in Compressive Spectral Imaging". In: *IEEE Trans. Image Process.* 23.4, pp. 1896–1908. ISSN: 1057-7149. DOI: 10.1109/TIP.2014.2310125.

Bai, H. et al. (2015). "Alternating Optimization of Sensing Matrix and Sparsifying Dictionary for Compressed Sensing". In: *IEEE Transactions on Signal Processing* 63.6, pp. 1581–1594. ISSN: 1053-587X. DOI: 10.1109/TSP.2015.2399864.

Barbero, Á. and S. Sra (2014). "Modular proximal optimization for multidimensional total-variation regularization". In: *ArXiv e-prints*. arXiv: 1411.0589 [stat.ML].

Bellante, G.J. et al. (2013). "Aerial detection of a simulated CO2 leak from a geologic sequestration site using hyperspectral imagery". In: *International Journal of Greenhouse Gas Control* 13, pp. 124–137. ISSN: 17505836. DOI: 10.1016/j.ijggc.2012.11.034.

Bioucas-Dias, J. M et al. (2013). "Hyperspectral Remote Sensing Data Analysis and Future Challenges". In: *IEEE Geosci. Remote Sens. Mag.* 1.2, pp. 6–36. ISSN: 2168-6831.

Boyd, S. et al. (2011). “Distributed Optimization and Statistical Learning via the Alternating Direction Method of Multipliers”. In: *Found. Trends Mach. Learn.* 3.1, pp. 1–122. ISSN: 1935-8237. DOI: 10.1561/2200000016.

Bras, N. B. et al. (2012). “An Alternating Direction Algorithm for Total Variation Reconstruction of Distributed Parameters”. In: *IEEE Transactions on Image Processing* 21.6, pp. 3004–3016. ISSN: 1057-7149. DOI: 10.1109/TIP.2012.2188033.

Candes, E. J. and M. B. Wakin (2008). “An Introduction To Compressive Sampling”. In: *IEEE Signal Process. Mag.* 25.2, pp. 21–30. ISSN: 1053-5888. DOI: 10.1109/MSP.2007.914731.

Cuadros, A. P. et al. (2015). “Coded aperture optimization for compressive X-ray tomosynthesis”. In: *Opt. Express* 23.25, pp. 32788–32802. DOI: 10.1364/OE.23.032788.

Fowler, J. E. (2009). “Compressive-Projection Principal Component Analysis”. In: *IEEE Transactions on Image Processing* 18.10, pp. 2230–2242. ISSN: 1057-7149. DOI: 10.1109/TIP.2009.2025089.

Green, Robert O et al. (1998). “Imaging Spectroscopy and the Airborne Visible/Infrared Imaging Spectrometer (AVIRIS)”. In: *Remote Sensing of Environment* 65.3, pp. 227–248. ISSN: 0034-4257. DOI: http://doi.org/10.1016/S0034-4257(98)00064-9.

Kunkel, B. et al. (1991). “ROSIS imaging spectrometer and its potential for ocean parameter measurements (airborne and space-borne)”. In: *Int. J. of Remote Sens.* 12.4, pp. 753–761. DOI: 10.1080/01431169108929691.

Lin, Xing et al. (2014). “Spatial-spectral encoded compressive hyperspectral imaging”. In: *ACM Trans. Graph.* 33.6, 233:1–233:11. ISSN: 0730-0301.

Lu, Guolan and Baowei Fei (2014). “Medical hyperspectral imaging: a review”. In: *Journal of biomedical optics* 19.1, p. 10901. ISSN: 1560-2281. DOI: 10.1117/1.JBO.19.1.010901.

Luo, Xiaoyan et al. (2010). “Classification-based image-fusion framework for compressive imaging”. In: *Journal of Electronic Imaging* 19.3, pp. 033009–033009–14. DOI: 10.1117/1.3478879.

Martín, G., J. M. Bioucas-Dias, and A. Plaza (2015). “HYCA: A New Technique for Hyperspectral Compressive Sensing”. In: *IEEE Transactions on Geoscience and Remote Sensing* 53.5, pp. 2819–2831. ISSN: 0196-2892. DOI: 10.1109/TGRS.2014.2365534.

Medina, F., H.Arguello, and C. Gómez (2017). “A Quantitative and Qualitative Performance Analysis of Compressive Spectral Imagers”. In: *Revista Tecnura*.

Needell, D. and R. Ward (2013). “Stable Image Reconstruction Using Total Variation Minimization”. In: *SIAM Journal on Imaging Sciences* 6.2, pp. 1035–1058. DOI: 10.1137/120868281. eprint: http://dx.doi.org/10.1137/120868281.

Rubinstein, R., A. M. Bruckstein, and M. Elad (2010). “Dictionaries for Sparse Representation Modeling”. In: *Proceedings of the IEEE* 98.6, pp. 1045–1057. ISSN: 0018-9219. DOI: 10.1109/JPROC.2010.2040551.

Ryan, John et al. (2014). “Application of the Hyperspectral Imager for the Coastal Ocean to Phytoplankton Ecology Studies in Monterey Bay, CA, USA”. In: *Remote Sensing* 6.2, pp. 1007–1025. ISSN: 2072-4292. DOI: 10.3390/rs6021007.

Tosic, I. and P. Frossard (2011). “Dictionary Learning”. In: *IEEE Signal Processing Magazine* 28.2, pp. 27–38. ISSN: 1053-5888.

Wagadarikar, A. et al. (2008). “Single disperser design for coded aperture snapshot spectral imaging.” In: *Appl. Opt.* 47.10, B44–51. ISSN: 0003-6935.

Wei, Q., N. Dobigeon, and J. Y. Tourneret (2015). “Bayesian Fusion of Multi-Band Images”. In: *IEEE Journal of Selected Topics in Signal Processing* 9.6, pp. 1117–1127. ISSN: 1932-4553. DOI: 10.1109/JSTSP.2015.2407855.

Wei, Q. et al. (2015). “Hyperspectral and Multispectral Image Fusion Based on a Sparse Representation”. In: *IEEE Trans. Geosci. Remote Sens.* 53.7, pp. 3658–3668. ISSN: 0196-2892.

Wei, Q. et al. (2016). “High-resolution hyperspectral image fusion based on spectral unmixing”. In: *2016 19th International Conference on Information Fusion (FUSION)*, pp. 1714–1719.

Xiong, Zhenjie et al. (2014). “Applications of Hyperspectral Imaging in Chicken Meat Safety and Quality Detection and Evaluation: A Review”. In: *Critical reviews in food science and nutrition*, null. ISSN: 1549-7852. DOI: 10.1080/10408398.2013.834875.

Yin, Hongpeng et al. (2015). “A novel image fusion approach based on compressive sensing”. In: *Optics Communications* 354, pp. 299 –313. ISSN: 0030-4018. DOI: http://dx.doi.org/10.1016/j.optcom.2015.05.020.